Femto-Photography: Capturing and Visualizing the Propagation of Light

Andreas Velten[1*] Di Wu[1†] Adrian Jarabo[2] Belen Masia[1,2] Christopher Barsi[1]
Chinmaya Joshi[1‡] Everett Lawson[1] Moungi Bawendi[3] Diego Gutierrez[2] Ramesh Raskar[1]

[1] MIT Media Lab [2] Universidad de Zaragoza [3] MIT Department of Chemistry

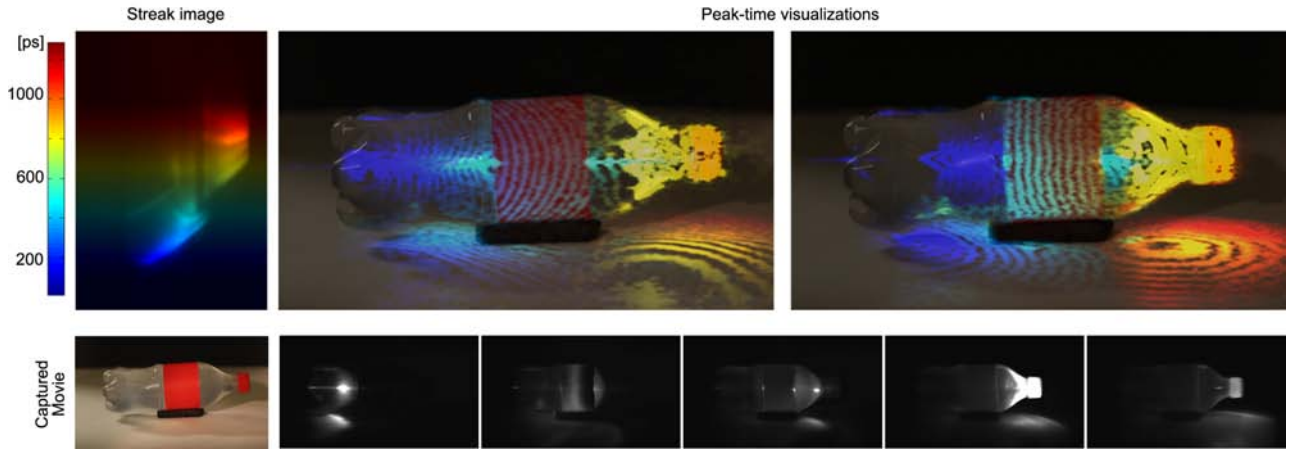

Figure 1: *What does the world look like at the speed of light? Our new computational photography technique allows us to visualize light in ultra-slow motion, as it travels and interacts with objects in table-top scenes. We capture photons with an effective temporal resolution of less than 2 picoseconds per frame. Top row, left: a false color, single streak image from our sensor. Middle: time lapse visualization of the bottle scene, as directly reconstructed from sensor data. Right: time-unwarped visualization, taking into account the fact that the speed of light can no longer be considered infinite (see the main text for details). Bottom row: original scene through which a laser pulse propagates, followed by different frames of the complete reconstructed video. For this and other results in the paper, we refer the reader to the video included in the supplementary material.*

Abstract

We present *femto-photography*, a novel imaging technique to capture and visualize the propagation of light. With an effective exposure time of 1.85 picoseconds (ps) per frame, we reconstruct movies of ultrafast events at an equivalent resolution of about one half trillion frames per second. Because cameras with this shutter speed do not exist, we re-purpose modern imaging hardware to record an ensemble average of repeatable events that are synchronized to a streak sensor, in which the time of arrival of light from the scene is coded in one of the sensor's spatial dimensions. We introduce reconstruction methods that allow us to visualize the propagation of femtosecond light pulses through macroscopic scenes; at such fast resolution, we must consider the notion of *time-unwarping* between the camera's and the world's space-time coordinate systems to take into account effects associated with the finite speed of light. We apply our femto-photography technique to visualizations of very different scenes, which allow us to observe the rich dynamics of time-resolved light transport effects, including scattering, specular reflections, diffuse interreflections, diffraction, caustics, and subsurface scattering. Our work has potential applications in artistic, educational, and scientific visualizations; industrial imaging to analyze material properties; and medical imaging to reconstruct subsurface elements. In addition, our time-resolved technique may motivate new forms of computational photography.

CR Categories: Computing Methodologies: Computer Graphics — Image Manipulation — Computational Photography

Keywords: ultrafast imaging, computational photography

Links: DL PDF WEB

1 Introduction

Forward and inverse analysis of light transport plays an important role in diverse fields, such as computer graphics, computer vision, and scientific imaging. Because conventional imaging hardware is slow compared to the speed of light, traditional computer graphics and computer vision algorithms typically analyze transport using low time-resolution photos. Consequently, any information that is encoded in the time delays of light propagation is lost. Whereas the joint design of novel optical hardware and smart computation, i.e, computational photography, has expanded the way we capture, ana-

*Currently at Morgridge Institute for Research, University of Wisconsin at Madison.

†Currently at Tsinghua University.

‡Currently at College of Engineering, Pune.

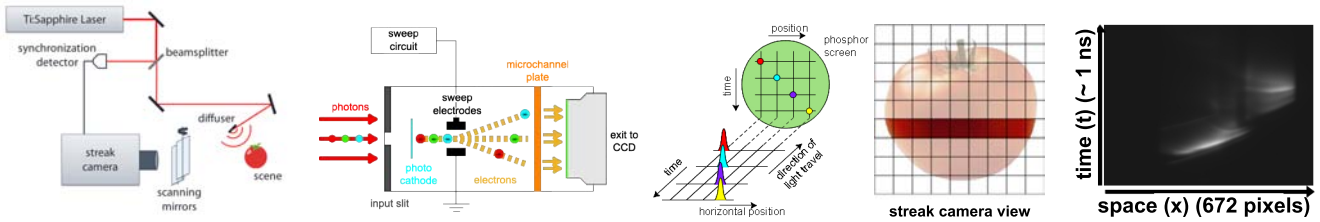

(a) (b) (c) (d) (e)

Figure 2: *Our setup for capturing a single 1D space-time photo. (a) A laser beam strikes a diffuser, which converts the beam into a spherical energy front that illuminates the scene; a beamsplitter and a synchronization detector enable synchronization between the laser and the streak sensor. (b) After interacting with the scene, photons enter a horizontal slit in the camera and strike a photocathode, which generates electrons. These are deflected at different angles as they pass through a microchannel plate, by means of rapidly changing the voltage between the electrodes. (c) The CCD records the horizontal position of each pulse and maps its arrival time to the vertical axis, depending on how much the electrons have been deflected. (d) We focus the streak sensor on a single narrow scan line of the scene. (e) Sample image taken by the streak sensor. The horizontal axis (672 pixels) records the photons' spatial locations in the acquired scanline, while the vertical axis (1 nanosecond window in our implementation) codes their arrival time. Rotating the adjustable mirrors shown in (a) allows for scanning of the scene in the y-axis and generation of ultrafast 2D movies such as the one visualized in Figure 1. (Figures (a)-(d), credit: [Gbur 2012])*

lyze, and understand visual information, speed-of-light propagation has been largely unexplored. In this paper, we present a novel ultrafast imaging technique, which we term *femto-photography*, consisting of femtosecond laser illumination, picosecond-accurate detectors, and mathematical reconstruction techniques, to allow us to visualize movies of light in motion as it travels through a scene, with an effective framerate of about one half trillion frames per second. This allows us to see, for instance, a light pulse scattering inside a plastic bottle, or image formation in a mirror, as a *function of time*.

Challenges Developing such time-resolved system is a challenging problem for several reasons that are under-appreciated in conventional methods: (a) brute-force time exposures under 2 ps yield an impractical signal-to-noise (SNR) ratio; (b) suitable cameras to record 2D image sequences at this time resolution do not exist due to sensor bandwidth limitations; (c) comprehensible visualization of the captured time-resolved data is non-trivial; and (d) direct measurements of events appear warped in space-time, because the finite speed of light implies that the recorded light propagation delay depends on camera position relative to the scene.

Contributions Our main contribution is in addressing these challenges and creating a first prototype as follows:

- We exploit the statistical similarity of periodic light transport events to record multiple, ultrashort exposure times of one-dimensional views (Section 3).
- We introduce a novel hardware implementation to sweep the exposures across a vertical field of view, to build 3D space-time data volumes (Section 4).
- We create techniques for comprehensible visualization, including movies showing the dynamics of real-world light transport phenomena (including reflections, scattering, diffuse inter-reflections, or beam diffraction) and the notion of *peak-time*, which partially overcomes the low-frequency appearance of integrated global light transport (Section 5).
- We introduce a *time-unwarping* technique to correct the distortions in captured time-resolved information due to the finite speed of light (Section 6).

Limitations Although not conceptual, our setup has several practical limitations, primarily due to the limited SNR of scattered light. Since the hardware elements in our system were originally designed for different purposes, it is not optimized for efficiency and suffers from low optical throughput (e.g., the detector is optimized for 500 nm visible light, while the infrared laser wavelength we use is 795 nm), and from dynamic range limitations. This lengthens the total recording time to approximately one hour. Furthermore, the scanning mirror, rotating continuously, introduces some blurring in the data along the scanned (vertical) dimension. Future optimized systems can overcome these limitations.

2 Related Work

Ultrafast Devices The fastest 2D continuous, real-time monochromatic camera operates at hundreds of nanoseconds per frame [Goda et al. 2009] (about $6 \cdot 10^6$ frames per second), with a spatial resolution of 200×200 pixels, less than one third of what we achieve. Avalanche photodetector (APD) arrays can reach temporal resolutions of several tens of picoseconds if they are used in a photon starved regime where only a single photon hits a detector within a time window of tens of nanoseconds [Charbon 2007]. Repetitive illumination techniques used in incoherent LiDAR [Tou 1995; Gelbart et al. 2002] use cameras with typical exposure times on the order of hundreds of picoseconds [Busck and Heiselberg 2004; Colaço et al. 2012], two orders of magnitude slower than our system. Liquid nonlinear shutters actuated with powerful laser pulses have been used to capture single analog frames imaging light pulses at picosecond time resolution [Duguay and Mattick 1971]. Other sensors that use a coherent phase relation between the illumination and the detected light, such as optical coherence tomography (OCT) [Huang et al. 1991], coherent LiDAR [Xia and Zhang 2009], light-in-flight holography [Abramson 1978], or white light interferometry [Wyant 2002], achieve femtosecond resolutions; however, they require light to maintain coherence (i.e., wave interference effects) during light transport, and are therefore unsuitable for indirect illumination, in which diffuse reflections remove coherence from the light. Simple streak sensors capture incoherent light at picosecond to nanosecond speeds, but are limited to a line or low resolution (20×20) square field of view [Campillo and Shapiro 1987; Itatani et al. 2002; Shiraga et al. 1995; Gelbart et al. 2002; Kodama et al. 1999; Qu et al. 2006]. They have also been used as line scanning devices for image transmission through highly scattering turbid media, by recording the ballistic photons, which travel a straight path through the scatterer and thus arrive first on the sensor [Hebden 1993]. The

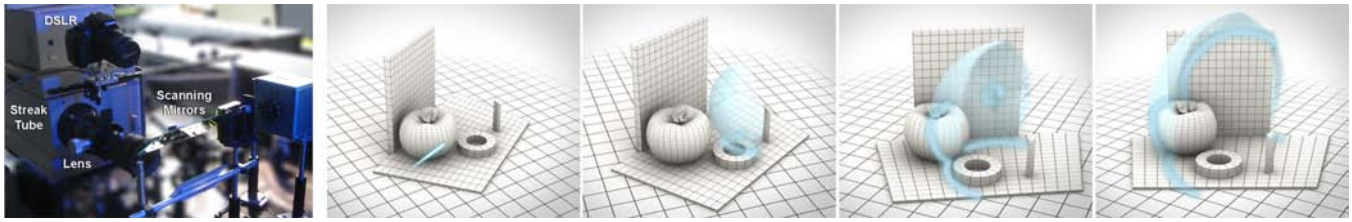

Figure 3: *Left: Photograph of our ultrafast imaging system setup. The DSLR camera takes a conventional photo for comparison. Right: Time sequence illustrating the arrival of the pulse striking a diffuser, its transformation into a spherical energy front, and its propagation through the scene. The corresponding captured scene is shown in Figure 10 (top row).*

principles that we develop in this paper for the purpose of transient imaging were first demonstrated by Velten et al. [2012c]. Recently, photonic mixer devices, along with nonlinear optimization, have also been used in this context [Heide et al. 2013].

Our system can record and reconstruct space-time world information of incoherent light propagation in free-space, table-top scenes, at a resolution of up to 672×1000 pixels and under 2 picoseconds per frame. The varied range and complexity of the scenes we capture allow us to visualize the *dynamics* of global illumination effects, such as scattering, specular reflections, interreflections, subsurface scattering, caustics, and diffraction.

Time-Resolved Imaging Recent advances in time-resolved imaging have been exploited to recover geometry and motion around corners [Raskar and Davis 2008; Kirmani et al. 2011; Velten et al. 2012b; Velten et al. 2012a; Gupta et al. 2012; Pandharkar et al. 2011] and albedo of from single view point [Naik et al. 2011]. But, none of them explored the idea of capturing videos of light in motion in direct view and have some fundamental limitations (such as capturing only third-bounce light) that make them unsuitable for the present purpose. Wu et al. [2012a] separate direct and global illumination components from time-resolved data captured with the system we describe in this paper, by analyzing the time profile of each pixel. In a recent publication [Wu et al. 2012b], the authors present an analysis on transient light transport in frequency space, and show how it can be applied to bare-sensor imaging.

3 Capturing Space-Time Planes

We capture time scales orders of magnitude faster than the exposure times of conventional cameras, in which photons reaching the sensor at different times are integrated into a single value, making it impossible to observe ultrafast optical phenomena. The system described in this paper has an effective exposure time down to 1.85 ps; since light travels at 0.3 mm/ps, light travels approximately 0.5 mm between frames in our reconstructed movies.

System: An ultrafast setup must overcome several difficulties in order to accurately measure a high-resolution (both in space and time) image. First, for an unamplified laser pulse, a single exposure time of less than 2 ps would not collect enough light, so the SNR would be unworkably low. As an example, for a table-top scene illuminated by a 100 W bulb, only about 1 photon on average would reach the sensor during a 2 ps open-shutter period. Second, because of the time scales involved, synchronization of the sensor and the illumination must be executed within picosecond precision. Third, standalone streak sensors sacrifice the vertical spatial dimension in order to code the time dimension, thus producing x-t images. As a consequence, their field of view is reduced to a single horizontal line of view of the scene.

We solve these problems with our ultrafast imaging system, outlined in Figure 2. (A photograph of the actual setup is shown in Figure 3 (left)). The light source is a femtosecond (fs) Kerr lens mode-locked Ti:Sapphire laser, which emits 50-fs with a center wavelength of 795 nm, at a repetition rate of 75 MHz and average power of 500 mW. In order to see ultrafast events in a scene with macro-scaled objects, we focus the light with a lens onto a Lambertian diffuser, which then acts as a point light source and illuminates the entire scene with a spherically-shaped pulse (see Figure 3 (right)). Alternatively, if we want to observe pulse propagation itself, rather than the interactions with large objects, we direct the laser beam across the field of view of the camera through a scattering medium (see the *bottle* scene in Figure 1).

Because all the pulses are statistically identical, we can record the scattered light from many of them and integrate the measurements to average out any noise. The result is a signal with a high SNR. To synchronize this illumination with the streak sensor (Hamamatsu C5680 [Hamamatsu 2012]), we split off a portion of the beam with a glass slide and direct it onto a fast photodetector connected to the sensor, so that, now, both detector and illumination operate synchronously (see Figure 2 (a)).

Capturing space-time planes: The streak sensor then captures an x-t image of a certain scanline (i.e. a line of pixels in the horizontal dimension) of the scene with a space-time resolution of 672×512. The exact time resolution depends on the amplification of an internal sweep voltage signal applied to the streak sensor. With our hardware, it can be adjusted from 0.30 ps to 5.07 ps. Practically, we choose the fastest resolution that still allows for capture of the entire duration of the event. In the streak sensor, a photocathode converts incoming photons, arriving from each spatial location in the scanline, into electrons. The streak sensor generates the x-t image by deflecting these electrons, according to the time of their arrival, to different positions along the t-dimension of the sensor (see Figure 2(b) and 2(c)). This is achieved by means of rapidly changing the sweep voltage between the electrodes in the sensor. For each horizontal scanline, the camera records a scene illuminated by the pulse and averages the light scattered by 4.5×10^8 pulses (see Figure 2(d) and 2(e)).

Performance Validation To characterize the streak sensor, we compare sensor measurements with known geometry and verify the linearity, reproducibility, and calibration of the time measurements. To do this, we first capture a streak image of a scanline of a simple scene: a plane being illuminated by the laser after hitting the diffuser (see Figure 4 (left)). Then, by using a Faro digitizer arm [Faro 2012], we obtain the ground truth geometry of the points along that plane and of the point of the diffuser hit by the laser; this allows us to compute the total travel time per path (diffuser-plane-streak sensor) for each pixel in the scanline. We then compare the travel time captured by our streak sensor with the real travel time computed

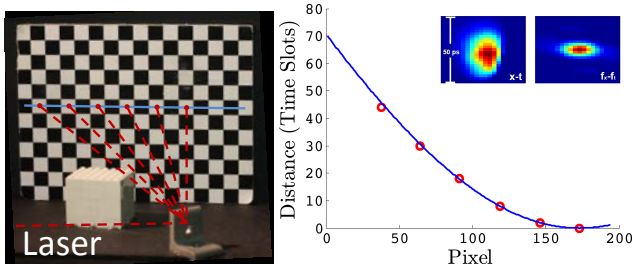

Figure 4: *Performance validation of our system. Left: Measurement setup used to validate the data. We use a single streak image representing a line of the scene and consider the centers of the white patches because they are easily identified in the data. Right: Graph showing pixel position vs. total path travel time captured by the streak sensor (red) and calculated from measurements of the checkerboard plane position with a Faro digitizer arm (blue). Inset: PSF, and its Fourier transform, of our system.*

from the known geometry. The graph in Figure 4 (right) shows agreement between the measurement and calculation.

4 Capturing Space-Time Volumes

Although the synchronized, pulsed measurements overcome SNR issues, the streak sensor still provides only a one-dimensional movie. Extension to two dimensions requires unfeasible bandwidths: a typical dimension is roughly 10^3 pixels, so a three-dimensional data cube has 10^9 elements. Recording such a large quantity in a 10^{-9} second (1 ns) time widow requires a bandwidth of 10^{18} byte/s, far beyond typical available bandwidths.

We solve this acquisition problem by again utilizing the synchronized repeatability of the hardware: A mirror-scanning system (two 9 cm $\times$ 13 cm mirrors, see Figure 3 (left)) rotates the camera's center of projection, so that it records horizontal slices of a scene sequentially. We use a computer-controlled, one-rpm servo motor to rotate one of the mirrors and consequently scan the field of view vertically. The scenes are about 25 cm wide and placed about 1 meter from the camera. With high gear ratios (up to 1:1000), the continuous rotation of the mirror is slow enough to allow the camera to record each line for about six seconds, requiring about one hour for 600 lines (our video resolution). We generally capture extra lines, above and below the scene (up to 1000 lines), and then crop them to match the aspect ratio of the physical scenes before the movie was reconstructed.

These resulting images are combined into one matrix, M_{ijk}, where $i = 1...672$ and $k = 1...512$ are the dimensions of the individual x-t streak images, and $j = 1...1000$ addresses the second spatial dimension y. For a given time instant k, the submatrix N_{ij} contains a two-dimensional image of the scene with a resolution of 672 $\times$ 1000 pixels, exposed for as short to 1.85 ps. Combining the x-t slices of the scene for each scanline yields a 3D x-y-t data volume, as shown in Figure 5 (left). An x-y slice represents one frame of the final movie, as shown in Figure 5 (right).

5 Depicting Ultrafast Videos in 2D

We have explored several ways to visualize the information contained in the captured x-y-t data cube in an intuitive way. First, contiguous N_{ij} slices can be played as the frames of a movie. Figure 1 (bottom row) shows a captured scene (*bottle*) along with several representative N_{ij} frames. (Effects are described for various scenes in Section 7.) However, understanding all the phenomena

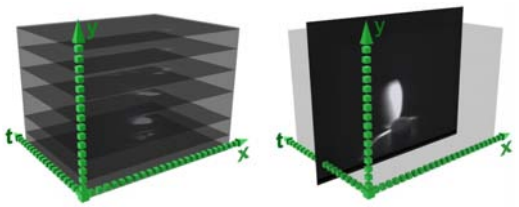

Figure 5: *Left: Reconstructed x-y-t data volume by stacking individual x-t images (captured with the scanning mirrors). Right: An x-y slice of the data cube represents one frame of the final movie.*

shown in a video is not a trivial task, and movies composed of x-y frames such as the ones shown in Figure 10 may be hard to interpret. Merging a static photograph of the scene from approximately the same point of view with the N_{ij} slices aids in the understanding of light transport in the scenes (see movies within the supplementary video). Although straightforward to implement, the high dynamic range of the streak data requires a nonlinear intensity transformation to extract subtle optical effects in the presence of high intensity reflections. We employ a logarithmic transformation to this end.

We have also explored single-image methods for intuitive visualization of full space-time propagation, such as the color-coding in Figure 1 (right), which we describe in the following paragraphs.

Integral Photo Fusion By integrating all the frames in novel ways, we can visualize and highlight different aspects of the light flow in one photo. Our photo fusion results are calculated as $N_{ij} = \sum w_k M_{ijk}, \{k = 1..512\}$, where w_k is a weighting factor determined by the particular fusion method. We have tested several different methods, of which two were found to yield the most intuitive results: the first one is *full fusion*, where $w_k = 1$ for all k. Summing all frames of the movie provides something resembling a black and white photograph of the scene illuminated by the laser, while showing time-resolved light transport effects. An example is shown in Figure 6 (left) for the *alien* scene. (More information about the scene is given in Section 7.) A second technique, *rainbow fusion*, takes the fusion result and assigns a different RGB color to each frame, effectively color-coding the temporal dimension. An example is shown in Figure 6 (middle).

Peak Time Images The inherent integration in fusion methods, though often useful, can fail to reveal the most complex or subtle behavior of light. As an alternative, we propose peak time images, which illustrate the time evolution of the *maximum* intensity in each frame. For each spatial position (i, j) in the x-y-t volume, we find the peak intensity along the time dimension, and keep information within two time units to each side of the peak. All other values in the streak image are set to zero, yielding a more sparse space-time volume. We then color-code time and sum up the x-y frames in this new sparse volume, in the same manner as in the *rainbow fusion* case but use only every 20th frame in the sum to create black lines between the equi-time paths, or isochrones. This results in a map of the propagation of maximum intensity contours, which we term *peak time image*. These color-coded isochronous lines can be thought of intuitively as propagating energy fronts. Figure 6 (right) shows the peak time image for the *alien* scene, and Figure 1 (top, middle) shows the captured data for the *bottle* scene depicted using this visualization method. As explained in the next section, this visualization of the bottle scene reveals significant light transport phenomena that could not be seen with the rainbow fusion visualization.

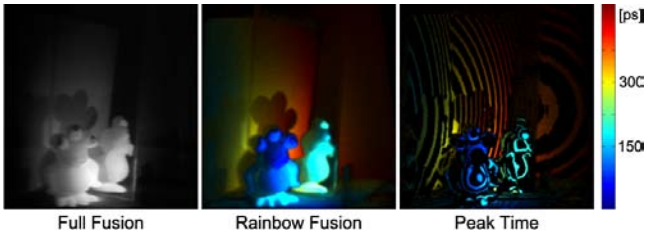

Figure 6: *Three visualization methods for the alien scene. From left to right, more sophisticated methods provide more information and an easier interpretation of light transport in the scene.*

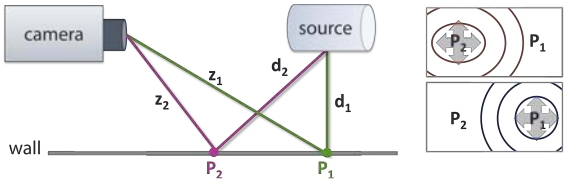

Figure 7: *Understanding reversal of events in captured videos. Left: Pulsed light scatters from a source, strikes a surface (e.g., at P_1 and P_2), and is then recorded by a sensor. Time taken by light to travel distances $z_1 + d_1$ and $z_2 + d_2$ is responsible for the existence of two different time frames and the need of computational correction to visualize the captured data in the world time frame. Right: Light appears to be propagating from P_2 to P_1 in camera time (before unwarping), and from P_1 to P_2 in world time, once time-unwarped. Extended, planar surfaces will intersect constant-time paths to produce either elliptical or circular fronts.*

6 Time Unwarping

Visualization of the captured movies (Sections 5 and 7) reveals results that are counter-intuitive to theoretical and established knowledge of light transport. Figure 1 (top, middle) shows a peak time visualization of the *bottle* scene, where several abnormal light transport effects can be observed: (1) the caustics on the floor, which propagate towards the bottle, instead of away from it; (2) the curved spherical energy fronts in the label area, which should be rectilinear as seen from the camera; and (3) the pulse itself being located behind these energy fronts, when it would need to precede them. These are due to the fact that usually light propagation is assumed to be infinitely fast, so that events in world space are assumed to be detected simultaneously in camera space. In our ultrafast photography setup, however, this assumption no longer holds, and the finite speed of light becomes a factor: we must now take into account the time delay between the occurrence of an event and its detection by the camera sensor.

We therefore need to consider two different time frames, namely *world time* (when events happen) and *camera time* (when events are detected). This duality of time frames is explained in Figure 7: light from a source hits a surface first at point $P_1 = (i_1, j_1)$ (with (i, j) being the x-y pixel coordinates of a scene point in the x-y-t data cube), then at the farther point $P_2 = (i_2, j_2)$, but the reflected light is captured in the reverse order by the sensor, due to different total path lengths ($z_1 + d_1 > z_2 + d_2$). Generally, this is due to the fact that, for light to arrive at a given time instant t_0, all the rays from the source, to the wall, to the camera, must satisfy $z_i + d_i = ct_0$, so that isochrones are elliptical. Therefore, although objects closer to the source receive light earlier, they can still lie on a higher-valued (later-time) isochrone than farther ones.

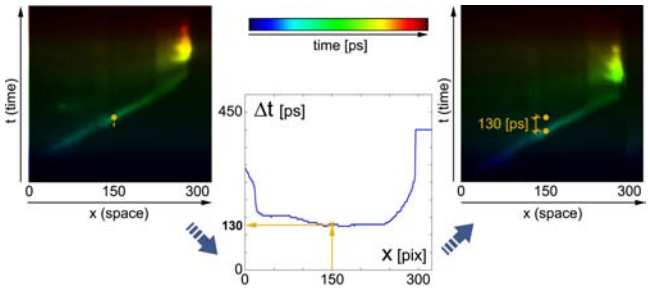

Figure 8: *Time unwarping in 1D for a streak image (x-t slice). Left: captured streak image; shifting the time profile down in the temporal dimension by Δt allows for the correction of path length delay to transform between time frames. Center: the graph shows, for each spatial location x_i of the streak image, the amount Δt_i that point has to be shifted in the time dimension of the streak image. Right: resulting time-unwarped streak image.*

In order to visualize all light transport events as they have occurred (not as the camera captured them), we transform the captured data from camera time to world time, a transformation which we term *time unwarping*. Mathematically, for a scene point $P = (i, j)$, we apply the following transformation:

$$t'_{ij} = t_{ij} + \frac{z_{ij}}{c/\eta} \tag{1}$$

where t'_{ij} and t_{ij} represent camera and world times respectively, c is the speed of light in vacuum, η the index of refraction of the medium, and z_{ij} is the distance from point P to the camera. For our table-top scenes, we measure this distance with a Faro digitizer arm, although it could be obtained from the data and the known position of the diffuser, as the problem is analogous to that of bi-static LiDAR. We can thus define light travel time from each point (i, j) in the scene to the camera as $\Delta t_{ij} = t'_{ij} - t_{ij} = z_{ij}/(c/\eta)$. Then, time unwarping effectively corresponds to offsetting data in the x-y-t volume along the time dimension, according to the value of Δt_{ij} for each of the (i, j) points, as shown in Figure 8.

In most of the scenes, we only have propagation of light through air, for which we take $\eta \approx 1$. For the *bottle* scene, we assume that the laser pulse travels along its longitudinal axis at the speed of light, and that only a single scattering event occurs in the liquid inside. We take $\eta = 1.33$ as the index of refraction of the liquid and ignore refraction at the bottle's surface. A step-by-step unwarping process is shown in Figure 9 for a frame (i.e. x-y image) of the *bottle* scene. Our unoptimized Matlab code runs at about 0.1 seconds per frame. A time-unwarped peak-time visualization of the whole of this scene is shown in Figure 1 (right). Notice how now the caustics originate from the bottle and propagate outward, energy fronts along the label are correctly depicted as straight lines, and the pulse precedes related phenomena, as expected.

7 Captured Scenes

We have used our ultrafast photography setup to capture interesting light transport effects in different scenes. Figure 10 summarizes them, showing representative frames and peak time visualizations. The exposure time for our scenes is between 1.85 ps for the *crystal* scene, and 5.07 ps for the *bottle* and *tank* scenes, which required imaging a longer time span for better visualization. Please refer to the video in the supplementary material to watch the reconstructed movies. Overall, observing light in such slow motion reveals both subtle and key aspects of light transport. We provide here brief

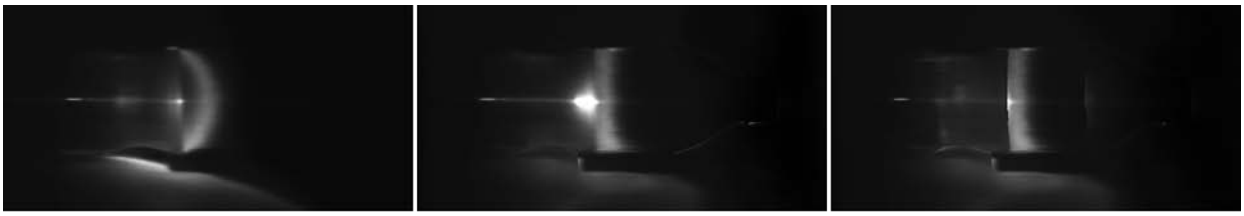

Figure 9: *Time unwarping for the bottle scene, containing a scattering medium. From left to right: a frame of the video without correction, where the energy front appears curved; the same frame after time-unwarping with respect to distance to the camera z_{ij}; the shape of the energy front is now correct, but it still appears before the pulse; the same frame, time-unwarped taking also scattering into account.*

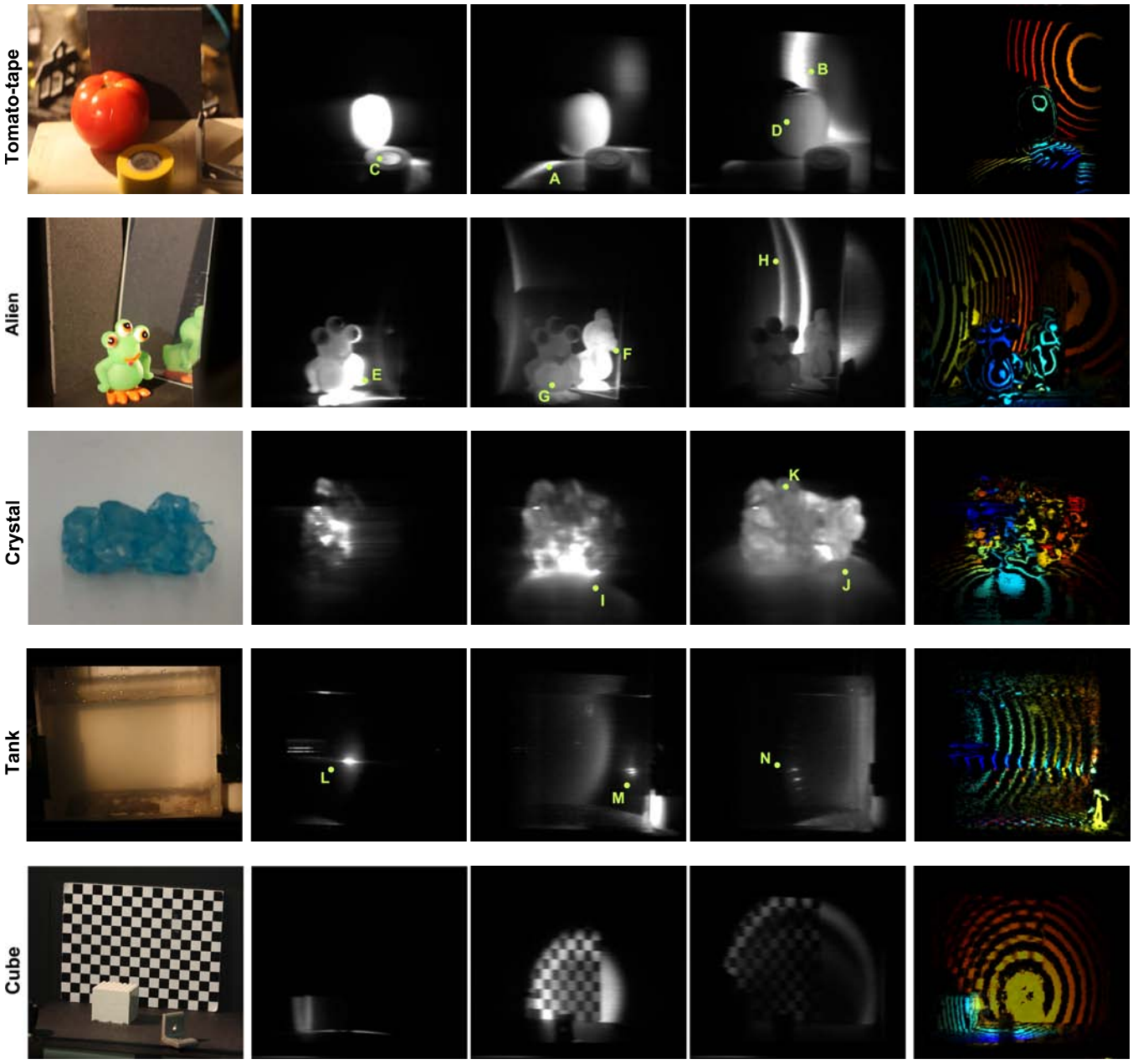

Figure 10: *More scenes captured with our setup (refer to Figure 1 for the bottle scene). For each scene, from left to right: photograph of the scene (taken with a DSLR camera), a series of representative frames of the reconstructed movie, and peak time visualization of the data. Please refer to the supplementary video the full movies. Note that the viewpoint varies slightly between the DSLR and the streak sensor.*

descriptions of the light transport effects captured in the different scenes.

Bottle This scene is shown in Figure 1 (bottom row), and has been used to introduce time-unwarping. A plastic bottle, filled with water diluted with milk, is directly illuminated by the laser pulse, entering through the bottom of the bottle along its longitudinal axis. The pulse scatters inside the liquid; we can see the propagation of the wavefronts. The geometry of the bottle neck creates some interesting lens effects, making light look almost like a fluid. Most of the light is reflected back from the cap, while some is transmitted or trapped in subsurface scattering phenomena. Caustics are generated on the table.

Tomato-tape This scene shows a tomato and a tape roll, with a wall behind them. The propagation of the spherical wavefront, after the laser pulse hits the diffuser, can be seen clearly as it intersects the floor and the back wall (A, B). The inside of the tape roll is out of the line of sight of the light source and is not directly illuminated. It is illuminated later, as indirect light scattered from the first wave reaches it (C). Shadows become visible only after the object has been illuminated. The more opaque tape darkens quickly after the light front has passed, while the tomato continues glowing for a longer time, indicative of stronger subsurface scattering (D).

Alien A toy alien is positioned in front of a mirror and wall. Light interactions in this scene are extremely rich, due to the mirror, the multiple interreflections, and the subsurface scattering in the toy. The video shows how the reflection in the mirror is actually formed: direct light first reaches the toy, but the mirror is still completely dark (E); eventually light leaving the toy reaches the mirror, and the reflection is dynamically formed (F). Subsurface scattering is clearly present in the toy (G), while multiple direct and indirect interactions between the wall and the mirror can also be seen (H).

Crystal A group of sugar crystals is directly illuminated by the laser from the left, acting as multiple lenses and creating caustics on the table (I). Part of the light refracted on the table is reflected back to the candy, creating secondary caustics on the table (J). Additionally, scattering events are visible within the crystals (K).

Tank A reflective grating is placed at the right side of a tank filled with milk diluted in water. The grating is taken from a commercial spectrometer, and consists of an array of small, equally spaced rectangular mirrors. The grating is blazed: mirrors are tilted to concentrate maximum optical power in the first order diffraction for one wavelength. The pulse enters the scene from the left, travels through the tank (L), and strikes the grating. The grating reflects and diffracts the beam pulse (M). The different orders of the diffraction are visible traveling back through the tank (N). As the figure (and the supplementary movie) shows, most of the light reflected from the grating propagates at the blaze angle.

Cube A very simple scene composed of a cube in front of a wall with a checkerboard pattern. The simple geometry allows for a clear visualization and understanding of the propagation of wavefronts.

8 Conclusions and Future Work

Our research fosters new computational imaging and image processing opportunities by providing incoherent time-resolved information at ultrafast temporal resolutions. We hope our work will inspire new research in computer graphics and computational photography, by enabling forward and inverse analysis of light transport, allowing for full scene capture of hidden geometry and materials, or for relighting photographs. To this end, captured movies and data of the scenes shown in this paper are available at `femtocamera.info`. This exploitation, in turn, may influence the rapidly emerging field of ultrafast imaging hardware.

The system could be extended to image in color by adding additional pulsed laser sources at different colors or by using one continuously tunable optical parametric oscillator (OPO). A second color of about 400 nm could easily be added to the existing system by doubling the laser frequency with a nonlinear crystal (about $1000). The streak tube is sensitive across the entire visible spectrum, with a peak sensitivity at about 450 nm (about five times the sensitivity at 800 nm). Scaling to bigger scenes would require less time resolution and could therefore simplify the imaging setup. Scaling should be possible without signal degradation, as long as the camera aperture and lens are scaled with the rest of the setup. If the aperture stays the same, the light intensity needs to be increased quadratically to obtain similar results.

Beyond the ability of the commercially available streak sensor, advances in optics, material science, and compressive sensing may bring further optimization of the system, which could yield increased resolution of the captured x-t streak images. Nonlinear shutters may provide an alternate path to femto-photography capture systems. However, nonlinear optical methods require exotic materials and strong light intensities that can damage the objects of interest (and must be provided by laser light). Further, they often suffer from physical instabilities.

We believe that mass production of streak sensors can lead to affordable systems. Also, future designs may overcome the current limitations of our prototype regarding optical efficiency. Future research can investigate other ultrafast phenomena such as propagation of light in anisotropic media and photonic crystals, or may be used in applications such as scientific visualization (to understand ultra-fast processes), medicine (to reconstruct subsurface elements), material engineering (to analyze material properties), or quality control (to detect faults in structures). This could provide radically new challenges in the realm of computer graphics. Graphics research can enable new insights via comprehensible simulations and new data structures to render light in motion. For instance, relativistic rendering techniques have been developed using our data, where the common assumption of constant irradiance over the surfaces does no longer hold [Jarabo et al. 2013]. It may also allow a better understanding of scattering, and may lead to new physically valid models, as well as spawn new art forms.

Acknowledgements

We would like to thank the reviewers for their insightful comments, and the entire Camera Culture group for their support. We also thank Greg Gbur for letting us use some of the images shown in Figure 2, Elisa Amoros for the 3D illustrations in Figures 3 and 4, and Paz Hernando and Julio Marco for helping with the video. This work was funded by the Media Lab Consortium Members, MIT Lincoln Labs and the Army Research Office through the Institute for Soldier Nanotechnologies at MIT, the Spanish Ministry of Science and Innovation through the *Mimesis* project, and the EU-funded projects *Golem* and *Verve*. Di Wu was supported by the National Basic Research Project (No.2010CB731800) of China and the Key Project of NSFC (No. 61120106003 and 60932007). Belen Masia was additionally funded by an FPU grant from the Spanish Ministry of Education and by an NVIDIA Graduate Fellowship. Ramesh Raskar was supported by an Alfred P. Sloan Research Fellowship and a DARPA Young Faculty Award.

References

ABRAMSON, N. 1978. Light-in-flight recording by holography. *Optics Letters 3*, 4, 121–123.

BUSCK, J., AND HEISELBERG, H. 2004. Gated viewing and high-accuracy three-dimensional laser radar. *Applied optics 43*, 24, 4705–4710.

CAMPILLO, A., AND SHAPIRO, S. 1987. Picosecond streak camera fluorometry: a review. *IEEE Journal of Quantum Electronics 19*, 4, 585–603.

CHARBON, E. 2007. Will avalanche photodiode arrays ever reach 1 megapixel? In *International Image Sensor Workshop*, 246–249.

COLAÇO, A., KIRMANI, A., HOWLAND, G. A., HOWELL, J. C., AND GOYAL, V. K. 2012. Compressive depth map acquisition using a single photon-counting detector: Parametric signal processing meets sparsity. In *IEEE Computer Vision and Pattern Recognition, CVPR 2012*, 96–102.

DUGUAY, M. A., AND MATTICK, A. T. 1971. Pulsed-image generation and detection. *Applied Optics 10*, 2162–2170.

FARO, 2012. Faro Technologies Inc.: Measuring Arms. `http://www.faro.com`.

GBUR, G., 2012. A camera fast enough to watch light move? `http://skullsinthestars.com/2012/01/04/a-camera-fast-enough-to-watch-light-move/`.

GELBART, A., REDMAN, B. C., LIGHT, R. S., SCHWARTZLOW, C. A., AND GRIFFIS, A. J. 2002. Flash lidar based on multiple-slit streak tube imaging lidar. SPIE, vol. 4723, 9–18.

GODA, K., TSIA, K. K., AND JALALI, B. 2009. Serial time-encoded amplified imaging for real-time observation of fast dynamic phenomena. *Nature 458*, 1145–1149.

GUPTA, O., WILLWACHER, T., VELTEN, A., VEERARAGHAVAN, A., AND RASKAR, R. 2012. Reconstruction of hidden 3D shapes using diffuse reflections. *Optics Express 20*, 19096–19108.

HAMAMATSU, 2012. Guide to Streak Cameras. `http://sales.hamamatsu.com/assets/pdf/catsandguides/e_streakh.pdf`.

HEBDEN, J. C. 1993. Line scan acquisition for time-resolved imaging through scattering media. *Opt. Eng. 32*, 3, 626–633.

HEIDE, F., HULLIN, M., GREGSON, J., AND HEIDRICH, W. 2013. Low-budget transient imaging using photonic mixer devices. *ACM Trans. Graph. 32*, 4.

HUANG, D., SWANSON, E., LIN, C., SCHUMAN, J., STINSON, W., CHANG, W., HEE, M., FLOTTE, T., GREGORY, K., AND PULIAFITO, C. 1991. Optical coherence tomography. *Science 254*, 5035, 1178–1181.

ITATANI, J., QUÉRÉ, F., YUDIN, G. L., IVANOV, M. Y., KRAUSZ, F., AND CORKUM, P. B. 2002. Attosecond streak camera. *Phys. Rev. Lett. 88*, 173903.

JARABO, A., MASIA, B., AND GUTIERREZ, D. 2013. Transient rendering and relativistic visualization. Tech. Rep. TR-01-2013, Universidad de Zaragoza, April.

KIRMANI, A., HUTCHISON, T., DAVIS, J., AND RASKAR, R. 2011. Looking around the corner using ultrafast transient imaging. *International Journal of Computer Vision 95*, 1, 13–28.

KODAMA, R., OKADA, K., AND KATO, Y. 1999. Development of a two-dimensional space-resolved high speed sampling camera. *Rev. Sci. Instrum. 70*, 625.

NAIK, N., ZHAO, S., VELTEN, A., RASKAR, R., AND BALA, K. 2011. Single view reflectance capture using multiplexed scattering and time-of-flight imaging. *ACM Trans. Graph. 30*, 6, 171:1–171:10.

PANDHARKAR, R., VELTEN, A., BARDAGJY, A., BAWENDI, M., AND RASKAR, R. 2011. Estimating motion and size of moving non-line-of-sight objects in cluttered environments. In *IEEE Computer Vision and Pattern Recognition, CVPR 2011*, 265–272.

QU, J., LIU, L., CHEN, D., LIN, Z., XU, G., GUO, B., AND NIU, H. 2006. Temporally and spectrally resolved sampling imaging with a specially designed streak camera. *Optics Letters 31*, 368–370.

RASKAR, R., AND DAVIS, J. 2008. 5D time-light transport matrix: What can we reason about scene properties? Tech. rep., MIT.

SHIRAGA, H., HEYA, M., MAEGAWA, O., SHIMADA, K., KATO, Y., YAMANAKA, T., AND NAKAI, S. 1995. Laser-imploded core structure observed by using two-dimensional x-ray imaging with 10-ps temporal resolution. *Rev. Sci. Instrum. 66*, 1, 722–724.

TOU, T. Y. 1995. Multislit streak camera investigation of plasma focus in the steady-state rundown phase. *IEEE Trans. Plasma Science 23*, 870–873.

VELTEN, A., FRITZ, A., BAWENDI, M. G., AND RASKAR, R. 2012. Multibounce time-of-flight imaging for object reconstruction from indirect light. In *Conference for Lasers and Electro-Optics*, OSA, CM2F.5.

VELTEN, A., WILLWACHER, T., GUPTA, O., VEERARAGHAVAN, A., BAWENDI, M. G., AND RASKAR, R. 2012. Recovering three-dimensional shape around a corner using ultrafast time-of-flight imaging. *Nature Communications 3*, 745.

VELTEN, A., WU, D., JARABO, A., MASIA, B., BARSI, C., LAWSON, E., JOSHI, C., GUTIERREZ, D., BAWENDI, M. G., AND RASKAR, R. 2012. Relativistic ultrafast rendering using time-of-flight imaging. In *ACM SIGGRAPH Talks*.

WU, D., O'TOOLE, M., VELTEN, A., AGRAWAL, A., AND RASKAR, R. 2012. Decomposing global light transport using time of flight imaging. In *IEEE Computer Vision and Pattern Recognition, CVPR 2012*, IEEE, 366–373.

WU, D., WETZSTEIN, G., BARSI, C., WILLWACHER, T., O'TOOLE, M., NAIK, N., DAI, Q., KUTULAKOS, K., AND RASKAR, R. 2012. Frequency analysis of transient light transport with applications in bare sensor imaging. In *European Conference on Computer Vision, ECCV 2012*, Springer, 542–555.

WYANT, J. C. 2002. White light interferometry. In *SPIE*, vol. 4737, 98–107.

XIA, H., AND ZHANG, C. 2009. Ultrafast ranging lidar based on real-time Fourier transformation. *Optics Letters 34*, 2108–2110.